NANO LETTERS

pubs.acs.org/NanoLett Letter

# Down-Scalable and Ultra-fast Memristors with Ultra-high Density Three-Dimensional Arrays of Perovskite Quantum Wires

Swapnadeep Poddar, Yuting Zhang, Leilei Gu,[⊥] Daquan Zhang,[⊥] Qianpeng Zhang, Shuai Yan, Matthew Kam, Sifan Zhang, Zhitang Song, Weida Hu, Lei Liao, and Zhiyong Fan*

Cite This: *Nano Lett.* 2021, 21, 5036−5044 Read Online

ACCESS | Metrics & More | Article Recommendations | Supporting Information

**ABSTRACT:** With strikingly high speed, data retention ability and storage density, resistive RAMs have emerged as a forerunning nonvolatile memory. Here we developed a Re-RAM with ultra-high density array of monocrystalline perovskite quantum wires (QWs) as the switching matrix with a metallic silver conducting pathway. The devices demonstrated high ON/OFF ratio of ~$10^7$ and ultra-fast switching speed of ~100 ps which is among the fastest in literature. The devices also possess long retention time of over 2 years and record high endurance of ~6 × $10^6$ cycles for all perovskite Re-RAMs reported. As a concept proof, we have also successfully demonstrated a flexible Re-RAM crossbar array device with a metal−semiconductor−insulator−metal design for sneaky path mitigation, which can store information with long retention. Aggressive downscaling to ~14 nm lateral dimension produced an ultra-small cell effectively having 76.5 $nm^2$ area for single bit storage. Furthermore, the devices also exhibited unique optical programmability among the low resistance states.

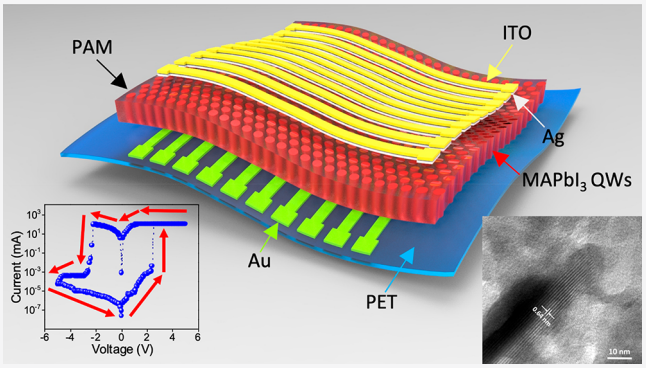


**KEYWORDS:** *perovskite quantum wires, resistive RAM, sub-ns switching speed, 14 nm lateral dimension, crossbar array*



## 1. INTRODUCTION

The ever-ascending evolution of a smarter world encompassing Internet of Things (IoT), neuromorphic computing, artificial intelligence, wearable electronics, and advanced healthcare demands a necessary up-gradation of the existing electronic memories. The fast-yet-volatile static random access memory (SRAM) and dynamic random access memory (DRAM) and nonevanescent-yet-fast FLASH memories are charge based systems that have reached their scalability limit due to enhanced quantum tunneling induced charge leakage at sub 10 nm scale.[1−3] As an alternative, nonvolatile memories (NVMs), particularly resistive RAMs (Re-RAMs) which store data in the form of distinct resistance levels with multibit storage capability, have taken the center-stage of scientific interest.[4,5] Among the different types of Re-RAMs, electrochemical-metalization cells (ECMs) have acquired tremendous attention because they are highly scalable and integrable.[6] Specifically, an ECM cell has a trilayered structure with a solid electrolyte sandwiched between an active electrode (AE) and an inert counter electrode (CE). The system switches from the high resistance state (HRS) to low resistance state (LRS) after a metallic filament of the AE material is electrochemically established between the AE and the CE. Most of the conventional solid electrolytes such as Cu-doped $SiO_2$, $ZrO_2$, etc. used in ECM cells require high temperature and sophisticated deposition processes.[7,8] In most cases these materials have been prepared in a continuous thin film (TF) form and thus the cross-talking among neighboring memory cells cannot be effectively eliminated.[9]

In fact, easy fabrication, inherent hysteresis and capability to accommodate ion migration, make hybrid perovskite materials ideal candidates for resistive memories.[10−14] In this work, we report an ECM Re-RAM using ultra-high density three-dimensional arrays of quantum wires (QWs) made of methylammonium lead iodide ($MAPbI_3$) perovskite as solid electrolyte and silver (Ag) as AE. The QWs have a diameter of ~10 nm approaching the exciton Bohr radius, thus demonstrating optical band-gap widening due to quantum confinement. Rigorous mechanistic study has confirmed that the electrical switching behavior in $MAPbI_3$ QWs and nanowires (NWs) originates from electrochemical reduction of Ag cation at aluminum (Al) CE and in body of QWs/NWs assisted by electron transport, leading to fast formation of Ag filament in material resulting in drastic conductivity increase. Switching speed measurement showed that the QW device has

**Received:** March 1, 2021
**Revised:** June 6, 2021
**Published:** June 14, 2021

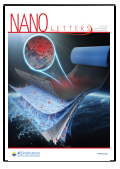





https://doi.org/10.1021/acs.nanolett.1c00834
*Nano Lett.* 2021, 21, 5036−5044

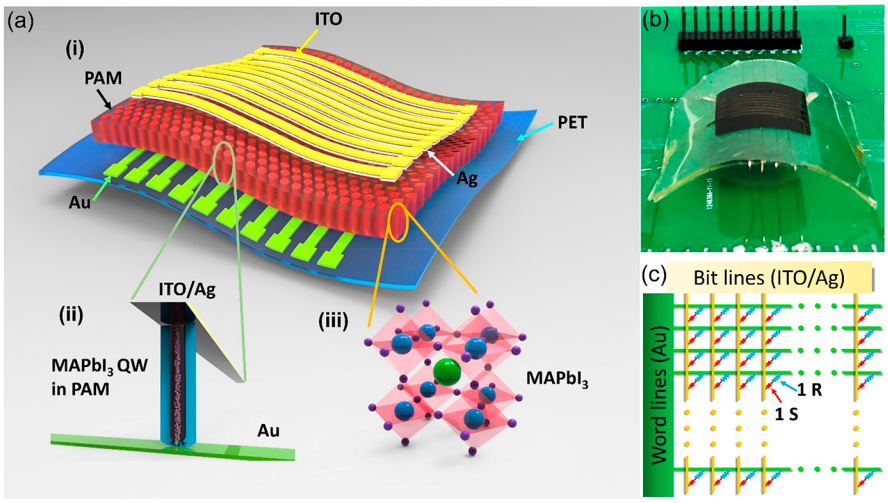


**Figure 1.** Device structure, photograph, and equivalent circuit of the QW memory device. (a) (i) Schematic showing the $MAPbI_3$ QWs/NWs in the PAM stacked between the crisscrossing Ag/ITO and Au finger electrodes, supported by a PET substrate. (ii) An enlarged view of an individual QW comprising the Ag filament sandwiched between ITO/Ag and Au contacts. (iii) Crytal strcuture of $MAPbI_3$. (b) Photograph of the flexible QW memory device. (c) Equivalent bitline−wordline circuit of the ITO/Ag/QW/Au memory device comprising the resistors, shown in blue (representing the QWs in LRS), and the selector, shown in red (MIM formed by $Ag/Al_2O_3/Au$), connected in series with the perovskite QWs in LRS.

100 ps programming speed, which is the fastest speed for all perovskite Re-RAM devices and nearly the record for all types of NVMs.[8,15−22] When encapsulated with UV curable epoxy, the memory devices showed extrapolated data retention of over 2 years and endurance performance of up to $6 \times 10^6$ cycles without any significant degradation in ON/OFF ratio. The devices comprising electrically isolated QWs with density up to $2 \times 10^{11}/cm^2$ demonstrated scalability down to ∼14 nm lateral dimension. Coupled with multibit storage, 76.5 $nm^2$ effective device area for single bit storage was obtained which is smaller than the effective single bit storage area of the state-of-the-art trilayered-cell (TLC) based 3D NAND and phase change memories (PCMs).[23] The device also responded to illumination, thus enabling optical programmability among different levels of LRSs. Eventually, a flexible cross-bar Re-RAM array that can alleviate the sneaky path issue and can store information with long retention, was demonstrated.

## 2. RESULTS AND DISCUSSION

Figure 1a shows the schematic of the ITO/Ag/$MAPbI_3$ QW (or NW)/Au flexible device. The $MAPbI_3$ QWs/NWs are grown with vapor phase method, as reported previously (Materials and Methods section).[24,25] They are embedded in the nanochannels of a porous alumina membrane (PAM) sandwiched by top and bottom electrodes. The material stack was attached on top of a polyethylene terephthalate (PET) substrate in order to instill flexibility to the system. Figure 1a also presents an enlarged view of a QW packaged in an individual nanochannel of the PAM with a thin aluminum oxide barrier layer between the QWs and the CE. An image of the actual memory device can be seen in Figure 1b. As can be seen in Figure 1c, the crossbar architectural model of our device comprises bit lines (ITO/Ag) and word lines (Au) with prevalent switching ($MAPbI_3$ QWs) and selecting ($Ag/Al_2O_3$/Au acting as a selecting metal−insulator−metal selector once device is SET) elements. This 1S-1R structure effectively suppresses cross-talk between neighboring cells.[9] X-ray diffraction (XRD) and scanning electron microscopy (SEM) of individual NWs/QWs can be found in Figure S1. Note that devices with Al as the CE instead of Au were used for carrying out all of the measurements that did not require a crossbar array architecture.

QWs with diameter of ∼10 nm and NWs with diameter of ∼250 nm were fabricated with periodicity of ∼25 and 500 nm, respectively. From Figure 2a, TEM investigation confirms single-crystallinity of a 9.5 nm diameter QW. The excitonic emission peak-shift from ∼780 nm for NWs to ∼725 nm for QWs shown in Figure 2b confirms energy band-gap widening when material dimension approaches the Bohr radius, thereby exhibiting the quantum confinement effect.[26] Figure 2c shows the cyclic $I-V$ sweeps for a 2 $\mu$m long QW Re-RAM device with voltage 0 V → 5 V → −5 V → 0 V. The initial sweep yielded higher switching voltage compared to subsequent stabilized sweeps indicating conducting filament formation.[27] From the $I-V$ plots, a high ON/OFF ratio of $\sim 10^7$ was observed.

A set of detailed tests were performed to unveil the underlying switching mechanism in the QW/NW Re-RAM devices. It can be seen from Figure S2a,b that a blank PAM devoid of any QW/NW and a device without a barrier layer demonstrated switching and no switching respectively, thereby establishing the perovskite QW/NW as the instrumental switching medium. When the Ag AE was replaced by Au and iron (Fe) electrodes, the devices did not yield any switching within a voltage scan range of 0 V → 6 V → −6 V → 0 V. However, when the voltage scan range was increased to 0 V → 25 V → −25 V → 0 V, the Au electrode based device showed switching from HRS → LRS at 13 V and from LRS → HRS at −17 V, contrary to the 2.4 V and −2.2 V for Ag based device (see Figure S3a−d). A comparative statistical study of devices with Au and Ag as top electrodes confirmed the trend of reduced threshold programming field and smaller LRS values for the Ag based devices (see Figure S3e,f). In contrast to the Au based devices with iodide vacancy mediated switching, the Ag based devices showed lower threshold switching field, owing to the ease of migration of Ag ions and


https://doi.org/10.1021/acs.nanolett.1c00834
Nano Lett. 2021, 21, 5036−5044

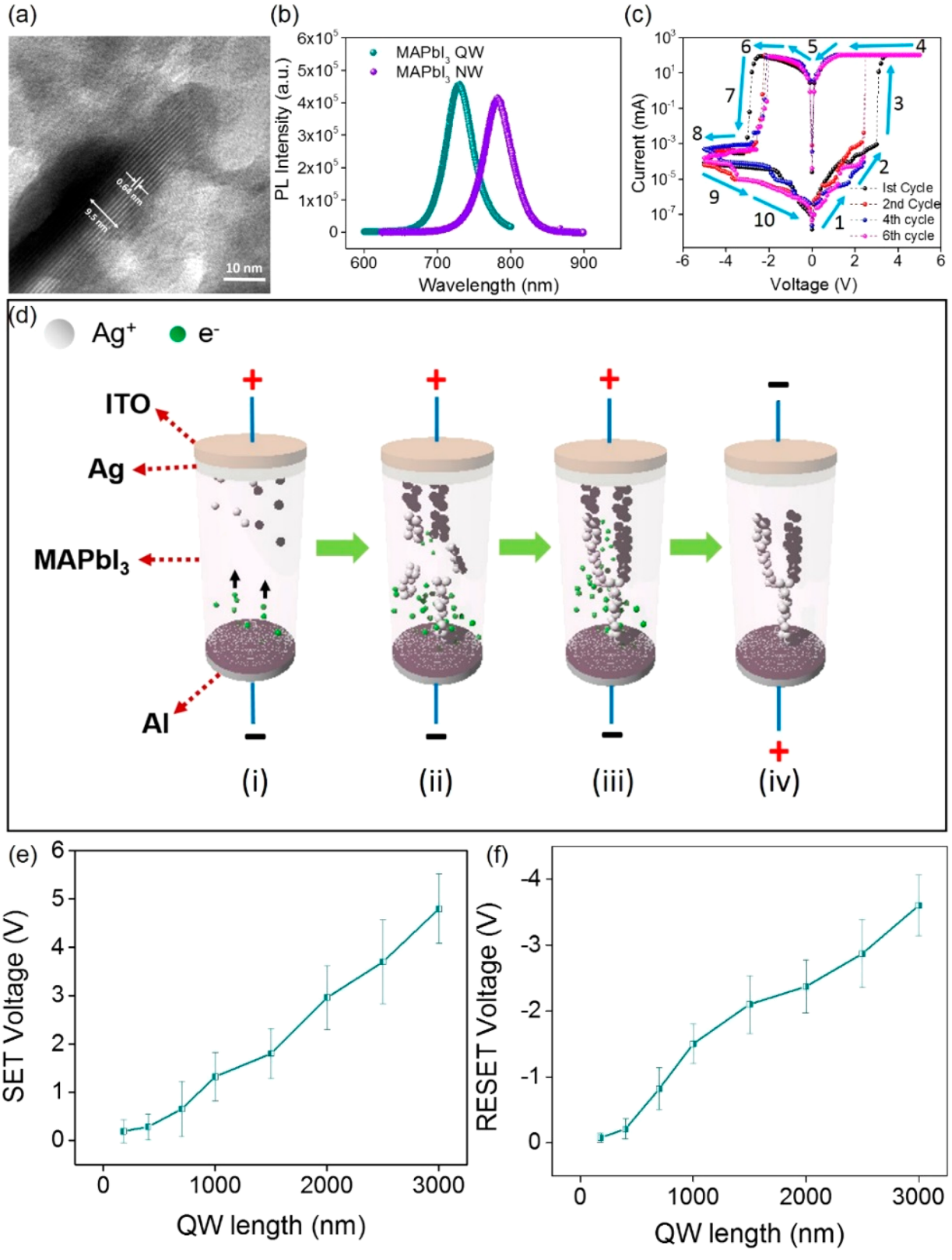


**Figure 2.** Structural, optical, and electrical characterization and working principle of QW memory device. (a) TEM image of 9.5 nm diameter QW. (b) Comparative photoluminescence spectrum of $MAPbI_3$ NW and QW. (c) $I-V$ sweeps of 2 $\mu$m long QW Re-RAM device. (d) Schematic illustrating the different stages of filament formation and rupture in the Re-RAM. (e) Plot showing the variation of SET voltage for different QW lengths. (f) Plot showing the variation of RESET voltage for different QW lengths.

the subsequent reduction to and supersaturation of metallic Ag by fast moving electrons in the monocrystalline QWs.[27−29] The large disparity in the ionic radii of Ag ions (110 pm) and iodide ions (220 pm) makes it difficult for iodide vacancies to be activated in a small voltage range thereby rendering the movement of Ag ions rather easier inside the perovskite NW/


https://doi.org/10.1021/acs.nanolett.1c00834
Nano Lett. 2021, 21, 5036−5044

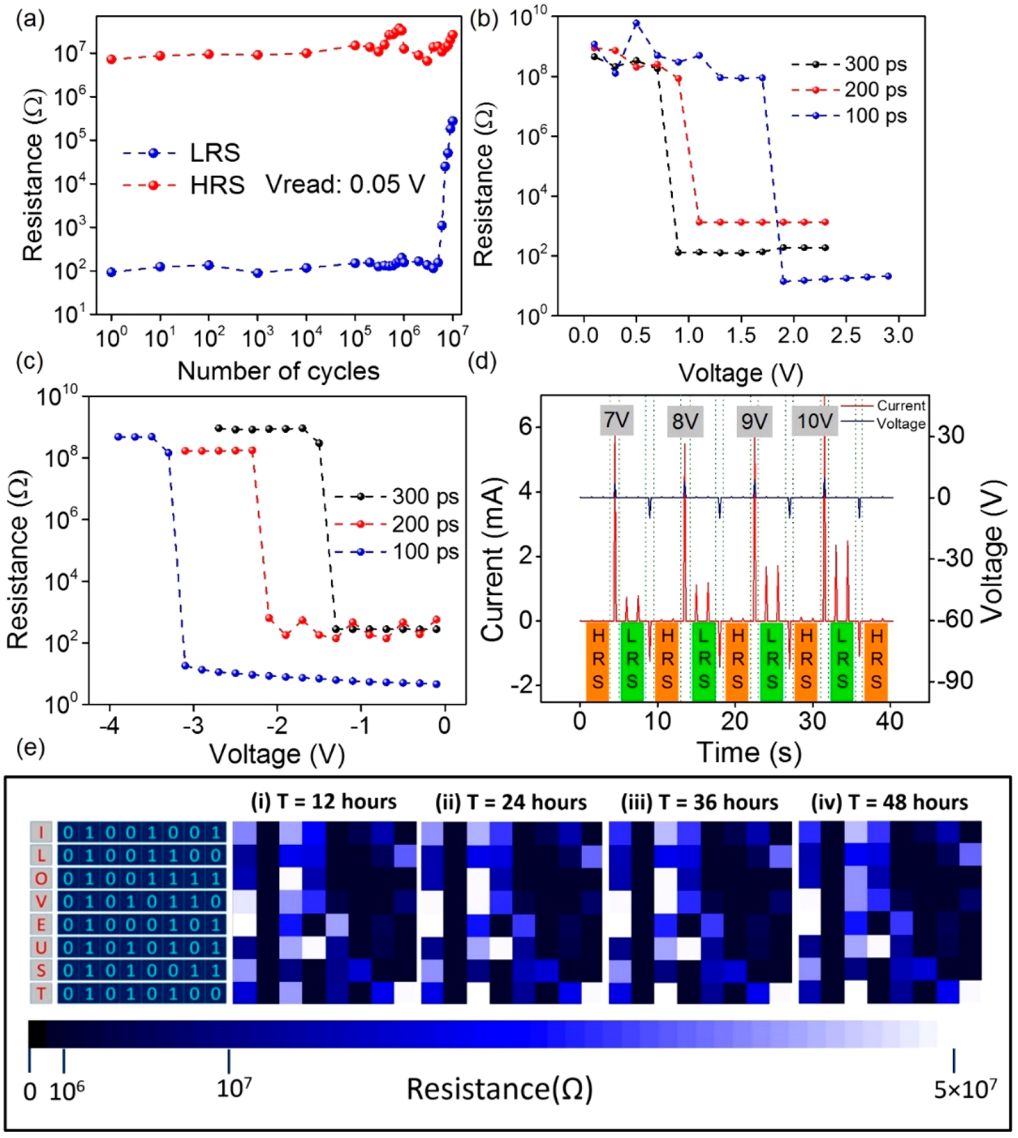


**Figure 3.** Endurance, switching time, multibit storage, and data retention of QW memory device. (a) Endurance study of the distinct resistance levels of the QW device exhibiting constancy of ON/OFF ratio and repeatability of the system. (b) Writing speed measurement for 180 nm long QW Re-RAM device exhibiting fastest speed of 100 ps. (c) Erasing speed measurement for 180 nm long QW Re-RAM device exhibiting fastest speed of 100 ps. (d) Plot showing the presence of multiple low resistance levels upon switching with writing voltage pulses of varying amplitude while reading and erasing with constant amplitude voltage pulses, all possessing width of 150 ms. (e) Matrix design illustrating the concept of alphabetic data storage and corresponding temporal retention of data. In accordance with the selector's readout window, a reading voltage of 0.15 V was used to read out resistances of the cells in the crossbar array.

QWs.[30] This rationale is further bolstered by the 2292 Ω and 11 Ω mean LRS values obatained for 40 Au and Ag based devices, respectively, which suggests that the conduction mechanism in the ON state for Ag based Re-RAMs is via metallic filament whereas it is nonmetallic for Au based devices.[31]

As can be seen from Figure S4a,b, when the polarity of the applied voltage was reversed, no switching was obtained for the first cycle but the consecutive cycles demonstrated writing on the negative side and erasing on the positive side. This proves that unless a positive voltage is applied to the Ag electrode (to oxidize Ag and repel $Ag^+$ into perovskite), the Ag pervasion into QW/NW is not triggered. Also, TEM studies with energy-dispersive X-ray spectroscopy (EDS) mappings on the pristine NWs (PNWs) and switched NWs (SNWs) yielded 2.76 atom % Ag for a SNW and 0.01 atom % Ag a PNW. Six such SNWs produced a mean atom % Ag of 2.49% (see Figure S5a,b and Table S1). In the quest of clinching evidence that can further bolster the theory of Ag pervasion, time of flight secondary mass ion spectroscopy (ToF-SIMS) was carried out on the pristine QWs and switched QWs (see Figure S6a–h). As demonstrated in Figure S6d, migration of Ag rendered a significantly higher intensity of secondary $CsAg^+$ ionic intensity for the switched devices compared to the pristine ones. Also, a single device in an array was selectively switched to LRS while the rest were made to stay in HRS. Ion-imaging for $CsAg^+$ normalized with respect to $Al^+$ performed at varying accumulated depths within the QW showed enhanced localized contrast for the device at LRS when compared to those at HRS (see Figure S6e–h). This inhomogeneous Ag filament based switching is in stark contrast to the traditional iodide vacancy mediated VCM (valence change memory)


https://doi.org/10.1021/acs.nanolett.1c00834
Nano Lett. 2021, 21, 5036−5044

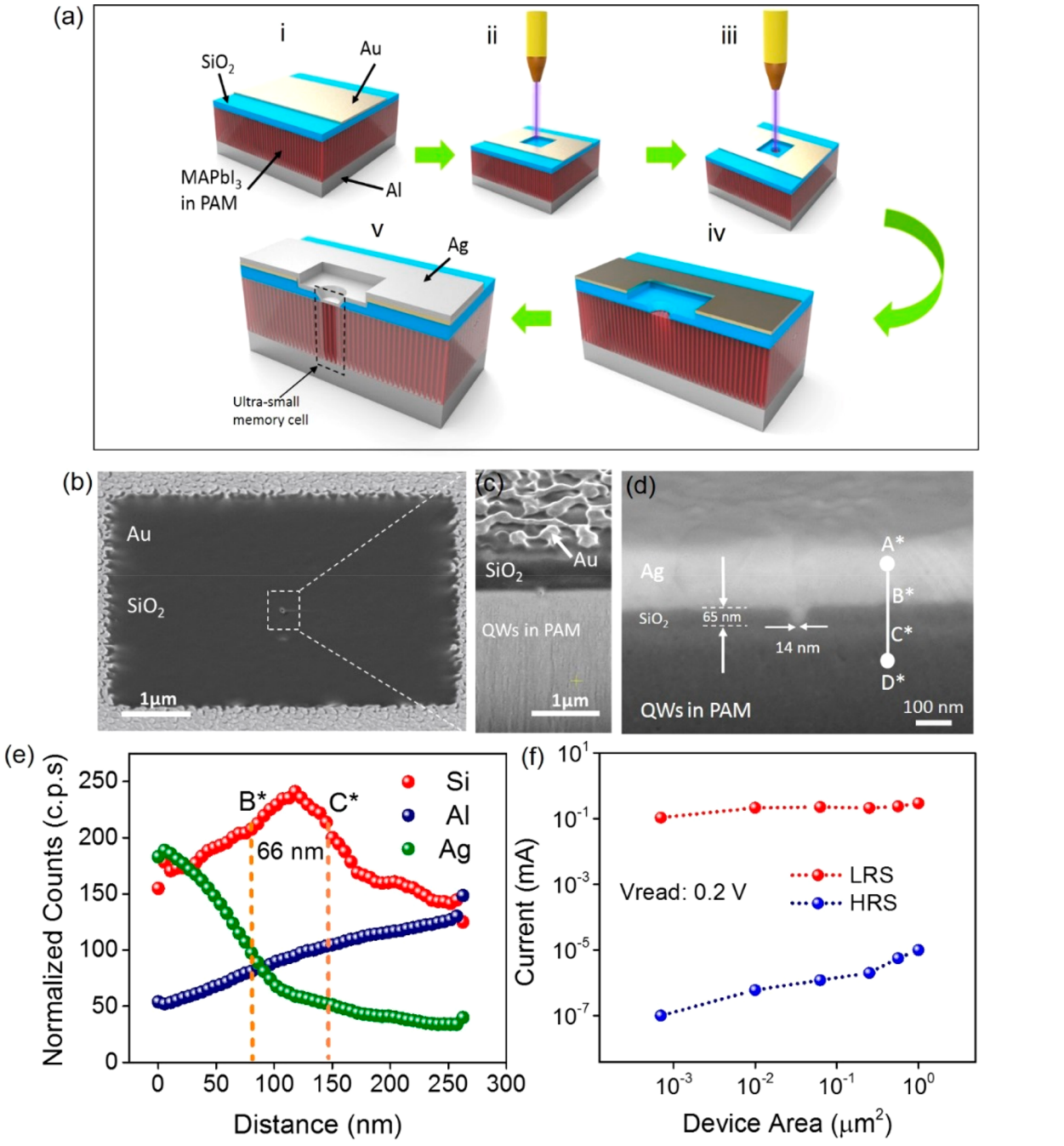


**Figure 4.** Downscaling of QW memory device. (a) Schematic illustrating the fabrication of ultra-small device using the focused ion beam. (b) Top view of 0.000 153 $\mu m^2$ (153 $nm^2$) device before Ag evaporation. (c) Cross-section of 0.000 153 $\mu m^2$ device before Ag evaporation. (d) Highly magnified cross-sectional view of 0.000 153 $\mu m^2$ device after Ag evaporation showing the distinct $SiO_2$ layer between the Ag electrode and $MAPbI_3$ QWs. (e) EDS line spectrum corresponding to Figure 4d exhibiting Si, Ag, and Al profile along the afore-portrayed cross-section. (f) Electrical response of the different small device sizes for the QW memory device fabricated by the FIB technique.

devices where homogeneous switching of the whole electrode area was reported with uniform distribution of surface potential.[32] It is also known that Ag electrodes suffer from stability issue after reacting with iodide-containing perovskite which has been observed in many TF devices.[33] However, our PAMs provide robust passivation for QWs/NWs, thus leading to drastically improved material and electrical stability, as shown in Supporting Information Figure S7.

Thus, the process of Ag conduction filament formation and rupture is schematically plotted in Figure 2d. According to the working principle of ECM memory,[34] once the positive voltage is applied to Ag electrode, the anodic dissolution of Ag takes place followed by the reduction of the electric-field driven $Ag^+$ to metallic Ag by fast moving electrons within the bulk of the monocrystalline QWs/NWs (Figure 2di). After the reduction process, nucleation succeeded by electrocrystallization and a fast growth of the Ag filament takes place toward the AE (Figure 2dii) with a rapid increase in QW/NW conductivity. The whole process is self-accelerating with ultra-fast switching speed. When Ag filaments bridge AE and CE (Figure 2diii), HRS to LRS switching is completed. Meanwhile, in the filament rupturing process (Figure 2div), when sufficient


https://doi.org/10.1021/acs.nanolett.1c00834
Nano Lett. 2021, 21, 5036−5044

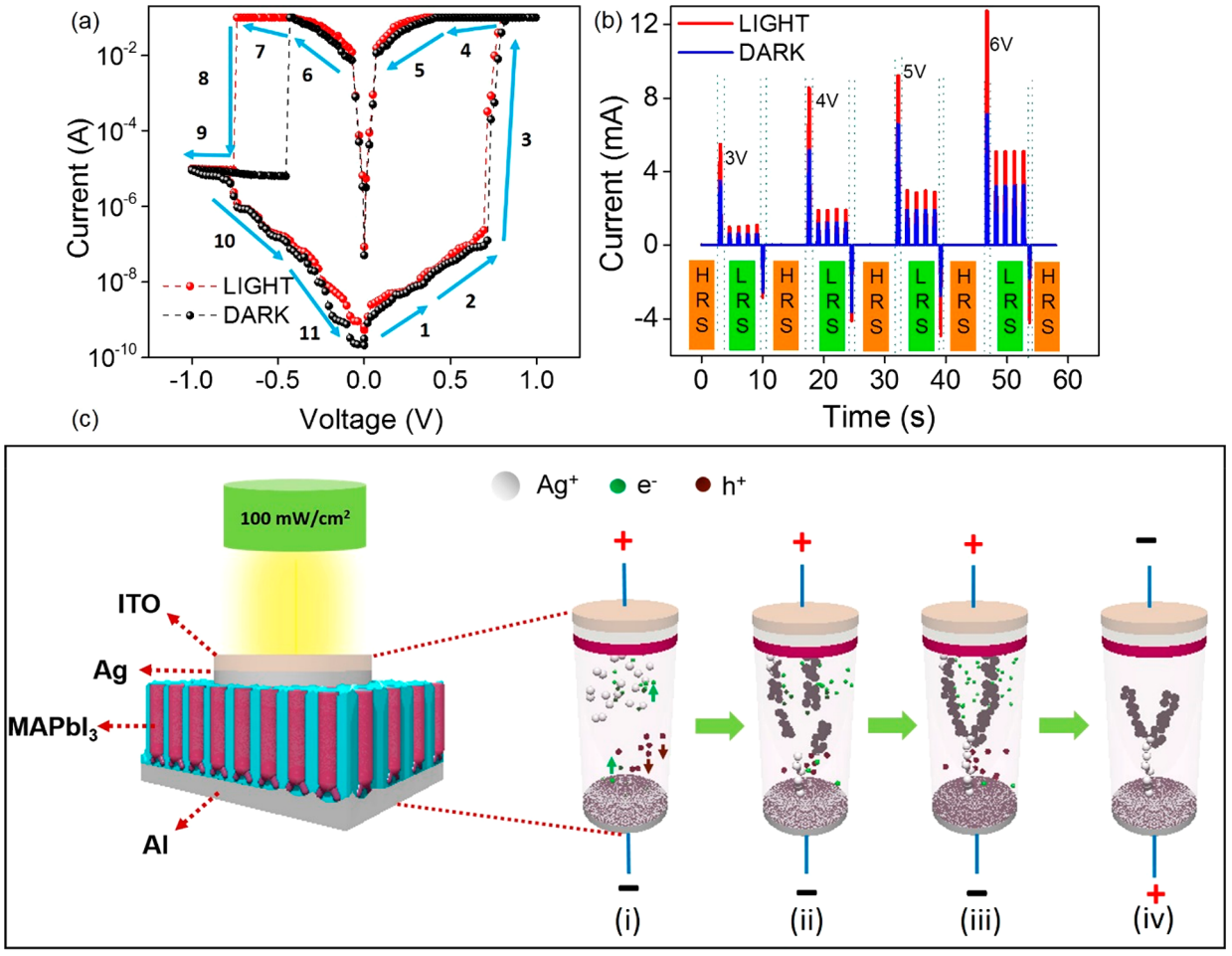


**Figure 5.** Light-response of NW memory device. (a) $I-V$ characteristics of the device exhibiting resistive switching under both dark and light conditions. (b) Multilevel switching behavior of the device after being SET in both light and dark while being subjected to 150 ms wide writing, reading, and erasing pulses of varying amplitude. (c) Schematic showing the resistive switching mechanism of the device when illuminated with light of intensity of 100 mW/cm$^2$.

negative voltage was applied to the Ag electrode, the effect of the counter-field coupled with Joule-heating resulted in the dissolution of the filament which became fragile at very high temperature (for thermal stability study of the LRS and HRS of QW Re-RAM, see Figure S8).

To explore the impact of QW/NW dimension on device performance, we tuned the wire length and observed intriguing relationship between programming voltage and wire length. Figure 2e,f, Figure S9, and Table S2 show the increasing trend of the switching voltage with increasing QW length. This particular dependence of the switching voltage on the QW length suggests that there is a threshold electric field that triggers electrical switching.[35] Details of variation of HRS and LRS current levels for NW/QW based Re-RAM have been provided in Figure S10a−d of Supporting Information. It must be mentioned that upon multiple cycles of switching, it was observed that the NW devices were more susceptible to enhancement of the HRS current compared to QW devices, rendering the latter to be more reliable for prolonged operation. This can be attributed to the fairly greater number of remnant Ag paths for electrons to traverse in the NWs due to its larger diameter compared to that of QWs (Figure S11 and Table S3).

Figure 3a shows the endurance of QW device packaged with a top layer of NOA 81 UV cured epoxy. At a reading voltage of 0.05 V, unhindered endurance performance of $6 \times 10^6$ cycles was obatined without any notable degradation in ON/OFF ratio, the highest reported for perovskite Re-RAM so far. The input pulse train with a single cycle current response and the cumulative probability plot of the maximum endurance, endurance of a TF device showing faster device failure and statistical study have been shown in Supporting Information Figure S12a−d. This attractive performance can be attributed to the unique protection mechanism provided by the robust PAM which was reported by us recently.[24,25,36]

To decipher the programming speed, the resistance of the QW/NW devices was traced with a 0.05 V reading voltage before and after the application of ultra-short pulses having a width as low as ∼100s of ps and maximum amplitude ∼7.5 V, a measurement technique reported previously.[18,19] The experimental setup and source pulses have been shown in Figure S13a−c. Shown in Figure 3b,c, the fastest writing and erasing speed obtained for the short QWs with length 180 nm was 100 ps at 1.7 V and −3.1 V, respectively, which is the record for all perovskite Re-RAMs and nearly the fastest reported speed in all NVM devices.[8,15−22] This ultra-fast switching speed can be explained by involving fast moving electrons to reduce $Ag^+$ cations in the body of the monocrystalline QWs. Study of QW length dependence on switching speed revealed that the shorter the QW length, faster was the speed which can be


https://doi.org/10.1021/acs.nanolett.1c00834
Nano Lett. 2021, 21, 5036−5044

attributed to the fact that with shorter length, Ag ions and electrons would traverse smaller distances for filament formation and rupture (see Figure S14a−d). Details of NW devices' switching speed, comparison of switching speed among different technologies, and statistical study have been shown in Figure S14e,f, Figures S15 and S16, and Tables S4 and S5, respectively. Note that the 180 nm long QW Re-RAM with ultra-fast switching speed, low switching voltage, and reliable HRS current level upon prolonged operation turned out to be the most energy efficient system. See Figure S17 and Tables S4 and S5 for detailed comparison with varying technologies.

The multibit data storage capability of the QW Re-RAM was demonstrated by feeding the device with continuous groups of read−write−read−erase−read voltage pulse strings. As shown in Figure 3d, 7 V, 8 V, 9 V, and 10 V writing voltages resulted in four LRSs with different distinct read currents of 1 mA, 1.2 mA, 1.8 mA, and 2.4 mA, respectively. Also, setting different current compliance values could regulate the filament formation after SET, thereby resulting in multiple levels of LRSs (see Figure S18). To characterize the retention time of the device, an 8 × 8 crossbar memory array using QWs embedded in a free-standing PAM was fabricated and the retention time of all 64 devices was examined at the same time. A string of letters, "I LOVE UST" were programmed into the memory device in the form of ASCII code with "0" and "1" representing HRS and LRS respectively (Figure 3e). Almost no degradation of data was observed over 48 h. With the aid of temperature accelerated tests, the retention time of an individual device was estimated to be 2.77 years at room temperature (RT) by using a readout voltage of 0.05 V (see Figure S23a,b). For details of sneaky path mitigation and comparison with TF devices, see Figures S19−S22, Table S6, and Figure S23c. The drastic improvement of retention time from 21 h in TF to over two years in QW devices is ascribed to the robust PAM passivation which prohibits moisture and oxygen assisted material degradation and filament oxidation.

To demonstrate the downscalability of QW Re-RAM comprising QWs of 10 nm diameter with ultra-high density of $2 \times 10^{11}/cm^2$, we fabricated ultra-small memory cells with lateral dimension of ∼14 nm and footprint of 153 $nm^2$ for at least two bit storage or effectively 76.5 $nm^2$ for 1 bit, which is already smaller than the state-of-the-art TLC based 64L NAND FLASH memory device.[23] Figure 4a schematically shows the device fabrication process. The key step is to form a nanometer scale via on the $SiO_2$ insulation layer covering QW array with focused-ion-beam (FIB) to allow subsequent Ag electrical point contact. Figure 4b,c shows the tilted angle view and cross-sectional view SEM of a device without top Ag electrode corresponding to step iv in Figure 4a. Figure 4d portrays the enlarged cross-sectional view of a completed device. The EDS line scan was performed to examine the profile of Si, Al, and Ag along the line A* − D*. Figure 4e demonstrates clearly device compositional change along line A*− D*. Figure 4f shows that although both LRS and HRS currents scale down monotonically with electrode size, HRS current scales down much faster than LRS current when reducing electrode size. Detailed discussion on comparison with other technologies and fabrication and characterization of the ultra-small devices have been provided in Figures S24−S31 and Tables S5 and S7.

$MAPbI_3$, due to its excellent optoelectronic properties, has been widely explored for photodetection and photovoltaics.[25,36−39] As shown in Figure 5a, 700 nm long NW device switching under 100 $mW/cm^2$ illumination showed enhancement in RESET voltage from −0.45 V to −0.75 V and a mean increase in LRS current by 54% . The photocurrent enhancement in HRS and the piecewise linear plots corresponding to Figure 5a have been shown in Figure S32a−i. Figure 5b shows that varying writing voltage pulse amplitude and keeping the illumination on only when writing led to 60% enhanced LRS current in read operation. As can be seen from the schematic in Figure 5ci, accompanying Ag atomic diffusion into $MAPbI_3$, Ag reacts with $MAPbI_3$ and forms a thin layer of AgI at the interface.[33] AgI is a photoresponsive material, and it decomposes into Ag and I under light illumination.[40] The photogenerated electrons together with injected electrons from CE significantly increase the $Ag^+$ cation reduction rate leading to extra Ag atoms driven into the system and formation of additional Ag in write/switching stage (Figure 5cii). Once the electrical contact is made by these filaments with the Ag electrode, switching to LRS is obtained (Figure 5ciii). When the light is turned off after switching, the additional Ag clusters or filaments enhanced the read current values even in the absence of light. In the RESET process, the additional negative voltage requirement can be ascribed to the additional energy required to rupture the extra filaments (Figure 5civ). Similarly, for QW devices, 70% increase in the erasing voltage and mean enhancement of 25% in LRS current were obtained when subjected to similar illumination tests (see Figure S32j,k).

## 3. CONCLUSION

In summary, we developed a Re-RAM with perovskite QW/NW arrays as the switching matrix possessing high ON/OFF ratio of $\sim 10^7$, multibit storage ability, ultra-fast programming speed of ∼100 ps, and excellent down-scalability to ∼14 nm lateral dimension with 76.5 $nm^2$ area for single bit storage. A proposed novel metal−semiconductor−insulator−metal scheme along with the PAM passivation to block lateral electrical leakages helped in addressing the sneaky path issue for a flexible crossbar device.The PAM passivation also instilled material stability to the devices resulting in drastically improved endurance and retention performance. These intriguing characteristics together demonstrate an attractive potency of perovskite QW Re-RAM devices as an alternative technology for future ultra-high density multi-functional NVMs with broad applications in integrated electronics, optoelectronics, and wearable devices.

## ■ ASSOCIATED CONTENT

### Supporting Information

The Supporting Information is available free of charge at https://pubs.acs.org/doi/10.1021/acs.nanolett.1c00834.

Materials and methods, structural and material characterizations, detailed mechanistic study (TEM, ToF-SIMS, and electrical characterizations), stability study on Re-RAM devices, detailed analysis of endurance, speed, and multilevel behavior, comparison study of figures-of-merit, sneaky path problem mitigation, down-scalability supporting data, and optical programmability (PDF)



https://doi.org/10.1021/acs.nanolett.1c00834
Nano Lett. 2021, 21, 5036−5044

## AUTHOR INFORMATION


### Corresponding Author

**Zhiyong Fan** − *Department of Electronic & Computer Engineering, The Hong Kong University of Science and Technology, Kowloon, Hong Kong SAR, China;* orcid.org/0000-0002-5397-0129; Email: eezfan@ust.hk

### Authors

**Swapnadeep Poddar** − *Department of Electronic & Computer Engineering, The Hong Kong University of Science and Technology, Kowloon, Hong Kong SAR, China*

**Yuting Zhang** − *Department of Electronic & Computer Engineering, The Hong Kong University of Science and Technology, Kowloon, Hong Kong SAR, China*

**Leilei Gu** − *Department of Electronic & Computer Engineering, The Hong Kong University of Science and Technology, Kowloon, Hong Kong SAR, China*

**Daquan Zhang** − *Department of Electronic & Computer Engineering, The Hong Kong University of Science and Technology, Kowloon, Hong Kong SAR, China*

**Qianpeng Zhang** − *Department of Electronic & Computer Engineering, The Hong Kong University of Science and Technology, Kowloon, Hong Kong SAR, China*

**Shuai Yan** − *State Key Laboratory of Functional Materials for Informatics, Shanghai Institute of Micro-system and Information Technology, Chinese Academy of Sciences, Shanghai 200050, China*

**Matthew Kam** − *Department of Electronic & Computer Engineering, The Hong Kong University of Science and Technology, Kowloon, Hong Kong SAR, China*

**Sifan Zhang** − *State Key Laboratory of Functional Materials for Informatics, Shanghai Institute of Micro-system and Information Technology, Chinese Academy of Sciences, Shanghai 200050, China*

**Zhitang Song** − *State Key Laboratory of Functional Materials for Informatics, Shanghai Institute of Micro-system and Information Technology, Chinese Academy of Sciences, Shanghai 200050, China*

**Weida Hu** − *State Key Laboratory of Infrared Physics, Shanghai Institute of Technical Physics, Chinese Academy of Sciences, Shanghai 200000, China;* orcid.org/0000-0001-5278-8969

**Lei Liao** − *Key Laboratory for Micro/Nano Optoelectronic Devices of Ministry of Education & Hunan Provincial Key Laboratory of Low-Dimensional Structural Physics and Devices, School of Physics and Electronics, Hunan University, Changsha 410082, China;* orcid.org/0000-0003-1325-2410

Complete contact information is available at: https://pubs.acs.org/10.1021/acs.nanolett.1c00834


### Author Contributions

[⊥]L.G and D.Z. contributed equally to this work. Z.F. and S.P. conceptualized the experiments and analyzed the results. Y.Z. performed the detailed high temperature retention time study. L.G. fabricated the flexible memory device. D.Z. performed the photoluminescence (PL) study for the quantum wires and nanowires and TEM image acquisition. Q.Z. acquired the high resolution SEM images for the ultra-small devices fabricated by focused ion beam technique. M.K. conducted fabrication and characterization of the thin film based memory devices. S.Y., S.Z., and Z.S. helped with the speed test for the memory device. W.H. and L.L. helped with device characterizations. All authors participated in manuscript writing and articulation.


### Funding

This work was supported by the National Natural Science Foundation of China (Project 51672231), the General Research Fund (Projects 16237816, 16309018, and 16214619) from the Hong Kong Research Grant Council, Innovation Technology Commission Fund (Project ITS/115/18), the HKUST Fund of Nanhai (Grant FSNH-18FYTRI01), Shenzhen Science and Technology Innovation Commission (Projects JCYJ20180306174923335 and JCYJ201708181141-07730).


### Notes

The authors declare no competing financial interest.

## ACKNOWLEDGMENTS


The authors thank Dr. Yuan Cai from Materials and Characterization Preparation Facility (MCPF) at HKUST for her help on focused ion beam operation, Dr. Roy Ho and Donald Y. K. Mak from HKUST MCPF for technically assisting in acquiring TEM images, and Prof. Lu Tao Weng from HKUST MCPF for assisting with the SIMS study. The authors thank Aashir Waleed, Jiaqi Chen, and Yu Fu for technical assistance. The authors also express gratitude to Amartansh Dubey at HKUST for help on LABVIEW programming. The authors thank all the funders of this work. The authors also acknowledge the support from the Center for 1D/2D Quantum Materials and State Key Laboratory of Advanced Displays and Optoelectronics.


## REFERENCES


(1) Meena, J. S.; Sze, S. M.; Chand, U.; Tseng, T.-Y. Overview of Emerging Nonvolatile Memory Technologies. *Nanoscale Res. Lett.* **2014**, *9* (1), 526.

(2) Jeong, D. S.; Thomas, R.; Katiyar, R.; Scott, J.; Kohlstedt, H.; Petraru, A.; Hwang, C. S. Emerging Memories: Resistive Switching Mechanisms and Current Status. *Rep. Prog. Phys.* **2012**, *75* (7), 076502.

(3) Wong, H.-S. P.; Salahuddin, S. Memory Leads the Way to Better Computing. *Nat. Nanotechnol.* **2015**, *10* (3), 191.

(4) Chang, T.-C.; Chang, K.-C.; Tsai, T.-M.; Chu, T.-J.; Sze, S. M. Resistance Random Access Memory. *Mater. Today* **2016**, *19* (5), 254−264.

(5) Cao, Q.; Lu, W.; Wang, X. R.; Guan, X.; Wang, L.; Yan, S.; Wu, T.; Wang, X. Nonvolatile Multistates Memories for High-Density Data Storage. *ACS Appl. Mater. Interfaces* **2020**, *12* (38), 42449−42471.

(6) Lu, W.; Jeong, D. S.; Kozicki, M.; Waser, R. Electrochemical Metallization Cells—Blending Nanoionics into Nanoelectronics? *MRS Bull.* **2012**, *37* (2), 124−130.

(7) Schindler, C.; Thermadam, S. C. P.; Waser, R.; Kozicki, M. N. Bipolar and Unipolar Resistive Switching in Cu-Doped $SiO_2$. *IEEE Trans. Electron Devices* **2007**, *54* (10), 2762−2768.

(8) Li, Y.; Long, S.; Zhang, M.; Liu, Q.; Shao, L.; Zhang, S.; Wang, Y.; Zuo, Q.; Liu, S.; Liu, M. Resistive Switching Properties of Au/$ZrO_2$/Ag Structure for Low-Voltage Nonvolatile Memory Applications. *IEEE Electron Device Lett.* **2010**, *31* (2), 117−119.

(9) Zidan, M. A.; Fahmy, H. A. H.; Hussain, M. M.; Salama, K. N. Memristor-based Memory: The Sneak Paths Problem and Solutions. *Microelectron. J.* **2013**, *44* (2), 176−183.

(10) Eames, C.; Frost, J. M.; Barnes, P. R.; O'regan, B. C.; Walsh, A.; Islam, M. S. Ionic Transport in Hybrid Lead Iodide Perovskite Solar Cells. *Nat. Commun.* **2015**, *6*, 7497.

(11) Xu, Z.; Liu, Z.; Huang, Y.; Zheng, G.; Chen, Q.; Zhou, H. To Probe the Performance of Perovskite Memory Devices: Defects Property and Hysteresis. *J. Mater. Chem. C* **2017**, *5* (23), 5810−5817.
(12) Guan, X.; Wang, Y.; Lin, C.-H.; Hu, L.; Ge, S.; Wan, T.; Younis, A.; Li, F.; Cui, Y.; Qi, D.-C.; et al. A monolithic artificial iconic memory based on highly stable perovskite-metal multilayers. *Appl. Phys. Rev.* **2020**, *7* (3), 031401.
(13) Ge, S.; Guan, X.; Wang, Y.; Lin, C. H.; Cui, Y.; Huang, Y.; Zhang, X.; Zhang, R.; Yang, X.; Wu, T. Low-Dimensional Lead-Free Inorganic Perovskites for Resistive Switching with Ultralow Bias. *Adv. Funct. Mater.* **2020**, *30* (25), 2002110.
(14) Younis, A.; Hu, L.; Sharma, P.; Lin, C. H.; Mi, Y.; Guan, X.; Zhang, D.; Wang, Y.; He, T.; Liu, X.; et al. Enhancing Resistive Switching Performance and Ambient Stability of Hybrid Perovskite Single Crystals via Embedding Colloidal Quantum Dots. *Adv. Funct. Mater.* **2020**, *30* (31), 2002948.
(15) Intel Optane Memory Series (16GB, M.2 80mm PCIe 3.0, 20nm, 3D Xpoint). https://ark.intel.com/products/97544/Intel-Optane-Memory-Series-16GB-M-2-80mm-PCIe-3-0-20nm-3D-Xpoint (accessed Dec 30, 2020).
(16) Dietrich, S.; Angerbauer, M.; Ivanov, M.; Gogl, D.; Hoenigschmid, H.; Kund, M.; Liaw, C.; Markert, M.; Symanczyk, R.; Altimime, L.; Bournat, S.; Mueller, G. A Nonvolatile 2-Mbit CBRAM Memory Core Featuring Advanced Read and Program Control. *IEEE J. Solid-State Circuits* **2007**, *42* (4), 839−845.
(17) Aratani, K.; Ohba, K.; Mizuguchi, T.; Yasuda, S.; Shiimoto, T.; Tsushima, T.; Sone, T.; Endo, K.; Kouchiyama, A.; Sasaki, S. A novel resistance memory with high scalability and nanosecond switching. *2007 IEEE International Electron Devices Meeting*; IEEE International, 2007; pp 783−786.
(18) Loke, D.; Lee, T.; Wang, W.; Shi, L.; Zhao, R.; Yeo, Y.; Chong, T.; Elliott, S. Breaking the Speed Limits of Phase-Change Memory. *Science* **2012**, *336* (6088), 1566−1569.
(19) Rao, F.; Ding, K.; Zhou, Y.; Zheng, Y.; Xia, M.; Lv, S.; Song, Z.; Feng, S.; Ronneberger, I.; Mazzarello, R.; Zhang, W.; Ma, E. Reducing the Stochasticity of Crystal Nucleation to Enable Subnanosecond Memory Writing. *Science* **2017**, *358* (6369), 1423−1427.
(20) Lee, H.; Chen, Y.; Chen, P.; Gu, P.; Hsu, Y.; Wang, S.; Liu, W.; Tsai, C.; Sheu, S.; Chiang, P. Evidence and solution of over-RESET problem for HfOx based resistive memory with sub-ns switching speed and high endurance. *2010 International Electron Devices Meeting*; IEEE, 2010; pp 19.7.1−19.7.4.
(21) Shukla, K. D.; Saxena, N.; Durai, S.; Manivannan, A. Redefining the Speed Limit of Phase Change Memory revealed by Time-resolved Steep Threshold-switching Dynamics of AgInSbTe devices. *Sci. Rep.* **2016**, *6*, 37868.
(22) Choi, B. J.; Torrezan, A. C.; Strachan, J. P.; Kotula, P.; Lohn, A.; Marinella, M. J.; Li, Z.; Williams, R. S.; Yang, J. J. High-speed and Low-energy nitride memristors. *Adv. Funct. Mater.* **2016**, *26* (29), 5290−5296.
(23) Choe, J. XPoint Memory Comparison Process & Architecture. Presented at Flash Memory Summit 2017, TechInsights, Santa Clara, CA, 2017.
(24) Waleed, A.; Tavakoli, M. M.; Gu, L.; Wang, Z.; Zhang, D.; Manikandan, A.; Zhang, Q.; Zhang, R.; Chueh, Y.-L.; Fan, Z. Lead-free Perovskite Nanowire Array Photodetectors with Drastically Improved Stability in Nanoengineering Templates. *Nano Lett.* **2017**, *17* (1), 523−530.
(25) Gu, L.; Tavakoli, M. M.; Zhang, D.; Zhang, Q.; Waleed, A.; Xiao, Y.; Tsui, K.-H.; Lin, Y.; Liao, L.; Wang, J.; Fan, Z. 3D Arrays of 1024-Pixel Image Sensors based on Lead Halide Perovskite Nanowires. *Adv. Mater.* **2016**, *28* (44), 9713−9721.
(26) Arbiol, J.; De La Mata, M.; Eickhoff, M.; i Morral, A. F. Bandgap Engineering in a Nanowire: Self-assembled 0, 1 and 2D Quantum Structures. *Mater. Today* **2013**, *16* (6), 213−219.
(27) Han, J. S.; Le, Q. V.; Choi, J.; Hong, K.; Moon, C. W.; Kim, T. L.; Kim, H.; Kim, S. Y.; Jang, H. W. Air-Stable Cesium Lead Iodide Perovskite for Ultra-Low Operating Voltage Resistive Switching. *Adv. Funct. Mater.* **2018**, *28* (5), 1705783.
(28) Gu, C.; Lee, J.-S. Flexible Hybrid Organic−inorganic Perovskite Memory. *ACS Nano* **2016**, *10* (5), 5413−5418.
(29) Hwang, B.; Lee, J.-S. Lead-free, Air-stable Hybrid Organic−inorganic Perovskite Resistive Switching Memory with Ultrafast Switching and Multilevel Data Storage. *Nanoscale* **2018**, *10* (18), 8578−8584.
(30) Shannon, R. D. Revised Effective Ionic Radii and Systematic Studies of Interatomic Distances in Halides and Chalcogenides. *Acta Crystallogr., Sect. A: Cryst. Phys., Diffr., Theor. Gen. Crystallogr.* **1976**, *32* (5), 751−767.
(31) Han, J. S.; Le, Q. V.; Choi, J.; Kim, H.; Kim, S. G.; Hong, K.; Moon, C. W.; Kim, T. L.; Kim, S. Y.; Jang, H. W. Lead-free all-inorganic cesium tin iodide perovskite for filamentary and interface-type resistive switching toward environment-friendly and temperature-tolerant nonvolatile memories. *ACS Appl. Mater. Interfaces* **2019**, *11* (8), 8155−8163.
(32) Solanki, A.; Guerrero, A.; Zhang, Q.; Bisquert, J.; Sum, T. C. Interfacial Mechanism for Efficient Resistive Switching in Ruddlesden−popper Perovskites for Non-volatile memories. *J. Phys. Chem. Lett.* **2020**, *11* (2), 463−470.
(33) Kato, Y.; Ono, L. K.; Lee, M. V.; Wang, S.; Raga, S. R.; Qi, Y. Silver Iodide Formation in Methyl Ammonium Lead Iodide Perovskite solar cells with Silver top electrodes. *Adv. Mater. Interfaces* **2015**, *2* (13), 1500195.
(34) Waser, R.; Dittmann, R.; Staikov, G.; Szot, K. Redox-based Resistive Switching Memories−nanoionic Mechanisms, Prospects, and Challenges. *Adv. Mater.* **2009**, *21* (25−26), 2632−2663.
(35) Ling, H.; Yi, M.; Nagai, M.; Xie, L.; Wang, L.; Hu, B.; Huang, W. Controllable Organic Resistive Switching Achieved by One-Step Integration of Cone-Shaped Contact. *Adv. Mater.* **2017**, *29* (35), 1701333.
(36) Waleed, A.; Fan, Z. Fabrication of Stable Organometallic Halide Perovskite NWs based Optoelectronic Devices. *Sci. Bull.* **2017**, *62* (9), 645−647.
(37) Waleed, A.; Tavakoli, M. M.; Gu, L.; Hussain, S.; Zhang, D.; Poddar, S.; Wang, Z.; Zhang, R.; Fan, Z. All Inorganic Cesium Lead Iodide Perovskite Nanowires with Stabilized Cubic Phase at Room Temperature and Nanowire Array-based Photodetectors. *Nano Lett.* **2017**, *17* (8), 4951−4957.
(38) Tavakoli, M. M.; Tsui, K.-H.; Zhang, Q.; He, J.; Yao, Y.; Li, D.; Fan, Z. Highly Efficient Flexible Perovskite Solar Cells with Antireflection and Self-cleaning Nanostructures. *ACS Nano* **2015**, *9* (10), 10287−10295.
(39) Mei, A.; Li, X.; Liu, L.; Ku, Z.; Liu, T.; Rong, Y.; Xu, M.; Hu, M.; Chen, J.; Yang, Y.; Gratzel, M.; Han, H. A Hole-conductor-free, Fully Printable Mesoscopic Perovskite Solar Cell with High Stability. *Science* **2014**, *345* (6194), 295−298.
(40) Belous, V. M.; Orlovskaya, N. A.; Akhmerov, A. Y.; Zenkevich, I. G.; Zhukov, S. A. In *Photodecomposition and Luminescence of Silver Halides*; PICS, 1999; pp 433−437.

## NOTE ADDED AFTER ASAP PUBLICATION

On June 23, 2021 two changes occurred, the sentence describing Figure S23d−f was removed from page 5042, and in the Supporting Information on page S53 a sentence was removed from before (k).


https://doi.org/10.1021/acs.nanolett.1c00834
*Nano Lett.* 2021, 21, 5036−5044